Available online at www.sciencedirect.com
ScienceDirect
Journal of Computational Physics 222 (2007) 110–130
JOURNAL OF COMPUTATIONAL PHYSICS
www.elsevier.com/locate/jcp

Dissipative particle dynamics simulation of fluid motion through an unsaturated fracture and fracture junction

Moubin Liu [a,b,*], Paul Meakin [a], Hai Huang [a]

[a] Center for Advanced Modeling and Simulation, Idaho National Laboratory, P.O. Box 1625, MS 2211, Idaho Falls, ID 83415-2211, United States
[b] College of Engineering, Nanyang Technological University, 50 Nanyang Avenue, Singapore 639798, Singapore

Received 21 April 2005; received in revised form 15 June 2006; accepted 3 July 2006
Available online 2 January 2007

Abstract

Multiphase fluid motion in unsaturated fractures and fracture networks involves complicated fluid dynamics, which is difficult to model using grid-based continuum methods. In this paper, the application of dissipative particle dynamics (DPD), a relatively new mesoscale method to simulate fluid motion in unsaturated fractures is described. Unlike the conventional DPD method that employs a purely repulsive conservative (non-dissipative) particle–particle interaction to simulate the behavior of gases, we used conservative particle–particle interactions that combine short-range repulsive and long-range attractive interactions. This new conservative particle–particle interaction allows the behavior of multiphase systems consisting of gases, liquids and solids to be simulated. Our simulation results demonstrate that, for a fracture with flat parallel walls, the DPD method with the new interaction potential function is able to reproduce the hydrodynamic behavior of fully saturated flow, and various unsaturated flow modes including thin film flow, wetting and non-wetting flow. During simulations of flow through a fracture junction, the fracture junction can be fully or partially saturated depending on the wetting property of the fluid, the injection rate and the geometry of the fracture junction. Flow mode switching from a fully saturated flow to a thin film flow can also be observed in the fracture junction.

Keywords: Dissipative particle dynamics (DPD); Smoothed particle hydrodynamics (SPH); Weight functions; Fracture; Fracture flow

1. Introduction

Unsaturated fractures in the vadose zone are very important for groundwater recharge, fluid motion and contaminant transport, and flow through fractures can lead to exceptionally rapid movement of liquids and associated contaminants [1–4]. The physics of fluid flows in unsaturated fractures is still poorly understood due to the complexity of multiple phase flow dynamics [5]. Experimental studies of fluid flow in fractures are limited [6,7], and in computer simulations it is usually difficult to take into account the fracture surface properties and microscopic roughness. Predictive numerical models can be divided into two general classes:

* Corresponding author. Tel.: +65 6514 1025; fax: +65 6791 1761.
E-mail address: liumb@ntu.edu.sg (M. Liu).

0021-9991/$ - see front matter © 2006 Published by Elsevier Inc.
doi:10.1016/j.jcp.2006.07.017

volume-averaged continuum models (such as those based on Richard's equation) [8] and discrete mechanistic models [9]. Knowledge of the physical properties of the fluids and the geometry of the fracture apertures is required in both classes. Volume-averaged continuum models are more suitable for large-scale systems, and they usually involve the representation of fractures as porous media with porosity and permeability parameters adjusted to mimic flow within fractures. However, volume-averaged continuum models are unable to describe the details of flow dynamics in fractures, they do not reproduce the spatio-temporal complexity of multiphase fluid flow in fractures, and they often fail to predict the rapid fluid motion and contaminant transport observed in the fractured vadose zone [10]. Small-scale studies with discrete mechanistic models are needed to develop a better understanding of the temporal and spatial dynamics of fracture flows. However, the complexity of fracture flow dynamics makes it difficult to develop successful numerical models for fluid flows in fracture networks. A broadly applicable model must be able to simulate a variety of phenomena including film flow with free surfaces, stable rivulets, snapping rivulets, fluid fragmentation and coalescence (including coalescence/fragmentation cascades), droplet migration and the formation of isolated single-phase islands trapped due to aperture variability [6].

Realistic mechanistic models for multiphase fracture flows must be able to handle moving interfaces, large density ratios (e.g., ≈1000:1 for water and air), and large viscosity ratios (e.g., ≈100:1 for water and air). These requirements combined with the complex geometries of natural fractures present severe challenges to mechanistic models. Grid-based numerical methods such as finite difference (FD) methods, finite volume (FV) methods and Eulerian finite element (FE) methods require special algorithms to treat and track the interface between different phases. These algorithms are usually complicated and fall into two general groups, interface tracking and interface capturing. Interface tracking algorithms generally use marker particles within grid cells intersected by the interface to identity the locations of interfaces [11,12]. The particles are then advected with the flow, and the positions of the interfaces can be determined from the particle positions. This approach is computationally expensive, especially for three-dimensional simulations [11,12], and often requires additional interface repairing techniques when the interface topology changes. Interface capturing algorithms are usually based on an 'indicator' field function with different values for different phases. The location of the interface can be determined from the indicator function, $f(\mathbf{x})$ where $\mathbf{x}$ is the position in the D-dimensional computational domain, which may have a specific value at the interface, or a range of values with a large gradient near the interface. The evolution of the moving interface can be obtained from the evolution of the indicator function. The volume of fluid (VOF) approach [13] is based on an indicator function that specifies how much fluid of each phase is contained in each of the grid cells. In the level-set (LS) function approach [14], the interface is a D-dimensional cut (contour) at $f = f^O$, through the $D+1$-dimensional surface $f(\mathbf{x})$. In most implementations, for two phase systems, $f(\mathbf{x})$ is positive in regions occupied by one phase, negative in regions occupied by the other, and $f^O = 0$. The VOF approach is robust and the mass loss/gain during a simulation is usually well controlled. But the captured interface usually spans several grid cells. In the LS approach, the interface is more sharply defined, but the loss/gain of mass during a simulation is larger.

Conventional grid based models such as FD, FV and FE models, which are based on continuum concepts and continuum equations such as the Navier–Stokes equation may not be accurate at small scales (e.g., mesoscale, microscale) fracture flows. On the other hand, molecular dynamics, which is in principle capable of providing reliable results on all scales, is practical only on extremely small time and length scales. A variety of particle-based 'mesoscale' models, which are much more computationally efficient than molecular dynamics, capture some of the characteristics of small scale systems such as thermally driven fluctuations, complex behaviors near fluid–fluid–solid contact lines and large fluid property gradients near solid surfaces. One well-known approach is the lattice-Boltzmann method [15–18] in which the motion of the particles is confined to the bonds of a regular lattice. Although this is a particle-based model, the motion of individual particles is not calculated explicitly. Instead, the model fluid is defined in terms of the particle velocity distribution function at every lattice node in the computational domain. The lattice-Boltzmann algorithm consists of alternating streaming and relaxation steps. In a streaming step particles move synchronously from each node to neighboring nodes, and in a relaxation step the velocity distributions at each node relaxes towards the discrete equilibrium distribution function corresponding to the local fluid velocity and density. Lattice-Boltzmann models have been applied to single phase flow and multiphase flow in fracture apertures [19]. Another approach is to use particle-based simulation methods, in which the individual particles represent a volume of fluid that may vary in size,

depending on the model, from a small cluster of atoms or molecules to an arbitrarily large macroscopic region. One example of this approach is the smoothed particle hydrodynamics (SPH) method, which was originally invented for astrophysical problems [20–22], and was recently extended to simulate three-dimensional fracture flows by Tartakovsky and Meakin [23,24]. In SPH, the state of a system is represented by a set of particles, which possess individual material properties and interact with each other within the range of a weight function (usually called the smoothing function in SPH). The discretization of the governing equations is based on these discrete particles, and a variety of particle-based formulations have been used to calculate the local density, velocity and acceleration of the fluid. In SPH simulations, the fluid pressure is calculated from the density using an equation of state, the particle acceleration is then calculated from the pressure gradient and the density. For low Reynolds number simulations the effects of viscosity on the particle accelerations are also included. As a Lagrangian particle method, SPH conserves mass exactly. In SPH, there is no explicit interface tracking – the motion of the fluid is represented by the motion of the particles, and fluid surfaces or fluid–fluid interfaces move with the particles. SPH methods for mesoscopic applications are still under development, and quantitative relationships between the model parameters used in SPH simulations and the macroscopic properties of the fluids that these models simulate are difficult to establish theoretically [24].

This paper describes the first effort to simulate fluid motion through unsaturated fracture apertures and fracture junctions using dissipative particle dynamics (DPD) [25]. DPD is a relatively new particle based mesoscale technique that can be used to simulate the behavior of fluids. DPD shares some features in common with SPH such as using particles to represent volumes of fluid. However, in DPD simulations the particle accelerations are calculated from pairwise particle–particle interactions (and viscous forces) instead of from the pressure gradient (and viscous forces). These two approaches to calculating particle accelerations are quite closely related because the particle acceleration obtained from the pressure gradient can also be obtained from particle–particle interactions calculated from the equation of state [26]. However these particle–particle interactions depend on the fluid density (they are many body, not pairwise, interactions). In DPD simulations, the particle–particle interactions consist of a 'conservative' (non-dissipative) component, a random (fluctuating) component and a dissipative component representing the effects of viscosity. The inclusion of random particle–particle interactions in addition to the conservative particle–particle interactions in DPD simulations is the most important feature that distinguishes DPD from SPH. The random particle–particle interactions generate fluctuations that correspond to thermally driven fluctuation in real fluids. These fluctuations are important only on microscopic physical scales. This makes DPD an essentially mesoscale (between the molecular and hydrodynamic scales) method, and the DPD fluid can be described by the continuum Navier–Stokes equation only on large scales (scales much greater than the particle size) on which the thermal fluctuations have a negligible effect. DPD facilitates the simulations of complex fluid systems on physically interesting and important length and time scales, and it rigorously conserves both the number of particles (equivalently, the total mass) and the total momentum of the system.

The conventional DPD method uses a simple linear function $1 - r$ as the weight function (or shape function) for the conservative force, where r is the distance between two DPD particles. This weight function describes a purely repulsive interaction, which is not able to simulate single component two phase (liquids/gas) fluids. It is possible to simulate two component two phase fluids [36] but it is not possible to simulate fluid pairs with large density contrasts. Therefore, conventional DPD with purely repulsive interactions is not able to model fracture flow phenomena which involve both liquids and gas phases or liquids with free surfaces. This paper uses an interaction potential consisting of a combination of attractive and repulsive bell-shaped functions (which are equivalent to the cubic spline smoothing functions frequently used in SPH simulations) with different interaction strengths and ranges. Particle–particle interactions of this form reflect the physical origins of single component fluids that can form coexisting liquid and gas phases. This paper shows that the DPD methods with these interaction potential functions are able to simulate single phase and two-phase fracture flows under a variety of flow conditions.

2. Dissipative particle dynamics

DPD was originally developed as an alternative to the lattice-Boltzmann method for simulating mesoscale fluids [19]. In the DPD method, a complex system can be simulated using a set of interacting particles. Each

particle represents a small cluster of atoms or molecules instead of a single molecule. Español and Warren [27] and Marsh [29] established a sound theoretical basis for DPD based on statistical mechanics. Since the introduction of the DPD method, it has been extended to many applications including colloidal suspensions [30], surfactants [31], dilute polymer solutions [32], biological membranes [33] and macromolecular movements [34].

2.1. Methodology

It is convenient to assume that all of the particles have equal masses, and use the mass of the particles as the unit of mass. Newton's second law governs the motion of each particle. The time evolution for a certain particle, i, is given by the equation of motion

$$\frac{\mathrm{d}\mathbf{r}_i}{\mathrm{d}t} = \mathbf{v}_i, \quad \frac{\mathrm{d}\mathbf{v}_i}{\mathrm{d}t} = \mathbf{f}_i = \mathbf{f}_i^{\mathrm{int}} + \mathbf{f}_i^{\mathrm{ext}}, \tag{1}$$

where $\mathbf{r}_i$ and $\mathbf{v}_i$ are the position and velocity vectors of particle i, $\mathbf{f}_i^{\mathrm{ext}}$ is the external force including the effects of gravity, and $\mathbf{f}_i^{\mathrm{int}}$ is the inter-particle force acting on particle i. The particle–particle interaction is usually assumed to be pairwise additive and consists of three parts: a conservative (non-dissipative) force, $\mathbf{F}_{ij}^{\mathrm{C}}$; a dissipative force, $\mathbf{F}_{ij}^{\mathrm{D}}$; and a random force, $\mathbf{F}_{ij}^{\mathrm{R}}$:

$$\mathbf{f}_i^{\mathrm{int}} = \sum_{j\neq i} \mathbf{F}_{ij} = \sum_{j\neq i} \mathbf{F}_{ij}^{\mathrm{C}} + \mathbf{F}_{ij}^{\mathrm{D}} + \mathbf{F}_{ij}^{\mathrm{R}}. \tag{2}$$

Here, $\mathbf{F}_{ij}$ is the inter-particle interaction force exerted on particle i by particle j, which is equal to $\mathbf{F}_{ji}$ in magnitude and opposite in direction. The symmetry of the interactions $\mathbf{F}_{ij} = -\mathbf{F}_{ji}$. ensures that momentum is rigorously conserved. The pairwise particle interactions have a finite cutoff distance, r_{c}, which is usually taken as the unit of length in DPD models.

The conservative force, $\mathbf{F}_{ij}^{\mathrm{C}}$, a "soft" interaction acting along the line of particle centers, has the form

$$\mathbf{F}_{ij}^{\mathrm{C}} = a_{ij} w^{\mathrm{C}}(r)\hat{\mathbf{r}}_{ij}, \tag{3}$$

where a_{ij} is the magnitude of the repulsive interaction between particles i and j, $\mathbf{r}_{ij} = \mathbf{r}_i - \mathbf{r}_j = |\mathbf{r}_{ij}|$, $\hat{\mathbf{r}}_{ij} = \mathbf{r}_{ij}/r_{ij}$ and $w^{\mathrm{C}}(r_{ij})$ is the weight function for the conservative force. Different weight functions can be used to describe different material properties.

The dissipative force $\mathbf{F}_{ij}^{\mathrm{D}}$ represents the effects of viscosity, and it depends on both the relative positions and velocities of the particles as

$$\mathbf{F}_{ij}^{\mathrm{D}} = -\gamma w^{\mathrm{D}}(r_{ij})(\mathbf{r}_{ij}\cdot\mathbf{v}_{ij})\mathbf{r}_{ij}, \tag{4}$$

where γ is a coefficient, $\mathbf{v}_{ij} = \mathbf{v}_i - \mathbf{v}_j$ and $w^{\mathrm{D}}(r_{ij})$ is the dissipation weight function.

The random force $\mathbf{F}_{ij}^{\mathrm{R}}$ represents the effects of thermal fluctuations and its dependence on the relative positions of the particles is given by

$$\mathbf{F}_{ij}^{\mathrm{R}} = \sigma w^{\mathrm{R}}(r_{ij})\xi_{ij}\hat{\mathbf{r}}_{ij}, \tag{5}$$

where σ is a coefficient, $w^{\mathrm{R}}(r_{ij})$ is the fluctuation weight function, and ξ_{ij} is a random variable. The random variable ξ_{ij} is selected from a Gaussian distribution with a zero mean and unit variance. In practice, random numbers that are uniformly distributed over a uniform range with a zero mean and unit variance can be used for ξ_{ij}.

The dissipative force and random force also act along the line of particle centers and therefore they also conserve linear and angular momentum.

Español and Warren [27] pointed out that in order to recover the proper thermodynamic equilibrium for a DPD fluid at a prescribed temperatures T, the coefficients and the weight functions for the random force and the dissipative force are not independent. The fluctuation–dissipation relationship [28] requires that

$$w^{\mathrm{D}}(r) = [w^{\mathrm{R}}(r)]^2 \tag{6}$$

and

$$\gamma = \frac{\sigma^2}{2k_B T}, \tag{7}$$

where k_B is the Boltzmann constant and T is the temperature. All of the interaction energies are expressed in units of $k_B T$, which is assigned a value of unity. One simple and straightforward choice for the dissipative and random weight functions is

$$w^D(r) = [w^R(r)]^2 = \begin{cases} (1-r)^2, & r < 1, \\ 0, & r \geqslant 1. \end{cases} \tag{8}$$

The random fluctuation force, $\mathbf{F}_{ij}^R$, acts to heat up the system (increases the average kinetic energy of the particles), whereas the dissipative force, $\mathbf{F}_{ij}^D$, acts to reduce the relative velocity of the particles, remove kinetic energy and cool down the system. The fluctuation–dissipation relationship described in Eqs. (6) and (7) ensures that the temperature calculated from the kinetic energy of the particles will remain constant.

The stress tensor, $\mathbf{S}$, is calculated using the Irving–Kirkwood model [35] expressed by the equation

$$\mathbf{S} = -\frac{1}{V}\left[\sum_i \mathbf{u}_i \mathbf{u}_i + \frac{1}{2}\sum_{i \neq j} \mathbf{r}_{ij}\mathbf{F}_{ij}\right], \tag{9}$$

where n is the number density of the particles, $\mathbf{u}_i = \mathbf{v}_i - \bar{\mathbf{v}}(\mathbf{r})$ is the peculiar velocity of particle i, $\bar{\mathbf{v}}(\mathbf{r})$ is the stream velocity at position $\mathbf{x}$. The first term in the brackets is the kinetic (ideal gas) contribution and the second term is the contribution from the particle–particle interactions. The pressure, p, is obtained from the trace of the stress tensor,

$$p = -\frac{1}{3}\mathrm{tr}\mathbf{S}. \tag{10}$$

The time integration algorithm is very important in DPD. Poor time integration algorithms lead to serious problems such as equilibrium properties that depend on the magnitude of the time step used. In the work described in this paper, a modified version of velocity-Verlet algorithm summarized by the equations

$$\begin{aligned} \mathbf{r}_i(t+\Delta t) &= \mathbf{r}_i(t) + \Delta t \mathbf{v}_i(t) + \frac{1}{2}(\Delta t)^2 \mathbf{f}_i(t), \\ \tilde{\mathbf{v}}_i(t+\Delta t) &= \mathbf{v}_i(t) + \lambda \Delta t \mathbf{f}_i(t), \\ \mathbf{f}_i(t+\Delta t) &= \mathbf{f}_i(\mathbf{r}_i(t+\Delta t), \tilde{\mathbf{v}}_i(t+\Delta t)), \\ \mathbf{v}_i(t+\Delta t) &= \mathbf{v}_i(t) + \frac{1}{2}\Delta t(\mathbf{f}_i(t) + \mathbf{f}_i(t+\Delta t)) \end{aligned} \tag{11}$$

was used to advance time [36], where $\tilde{\mathbf{v}}_i(t+\Delta t)$ is the prediction of the velocity of particle i at time $t+\Delta t$ and λ is an empirical parameter that accounts for some of the effects of the stochastic interactions [36]. In this time integration algorithm, the velocity is first predicted to obtain the force and then corrected in the last step while the force is calculated only once at each integration step.

2.2. SPH like interaction potentials

In typical DPD implementations, the weight function for the conservative force is given the form

$$w^C(r) = \begin{cases} (1-r), & r < 1.0, \\ 0, & r \geqslant 1.0. \end{cases} \tag{12}$$

This linear weight function describes a soft, purely repulsive interaction that forces the particles to separate from each other and occupy the entire computational domain.

This purely repulsive interaction is not able to model problems with co-existing liquid and gas phases such as multiphase flow problems in fractures. Based on the physical origins of single component fluids that can form coexisting liquid and gaseous phases, an interaction with short-range repulsion and long-range attraction is required to simulate multiphase fluid flow in unsaturated fractures.

A soft interaction with short-range repulsion and long-distance attraction can take a variety of forms. One straightforward approach is to use a combination of bell-shaped SPH smoothing functions with different interaction strengths and cut-off distances. The cubic spline function,

$$W(r) = W(r, r_c) = \begin{cases} 1 - \frac{3}{2}\left(\frac{2r}{r_c}\right)^2 + \frac{3}{4}\left(\frac{2r}{r_c}\right)^3, & 0 \leqslant \frac{2r}{r_c} < 1, \\ \frac{1}{4}\left(2 - \left(\frac{2r}{r_c}\right)\right)^3, & 1 \leqslant \frac{2r}{r_c} < 2, \\ 0, & \frac{2r}{r_c} \geqslant 2, \end{cases} \tag{13}$$

is the most commonly used smoothing function in SPH [37], where r_c is the cutoff distance (corresponding to the smoothing length h in SPH). For the cubic spline function, $r_c = 2h$. In SPH, the function $W(r)$ in Eq. (13) is multiplied by a coefficient, C, so that the normalization requirement $\int W(|r|)\mathrm{d}r = 1$ is satisfied. The normalization coefficient, C, has a value of $2/3h$, $10/7\pi h^2$ and $1/\pi h^3$ in the one-, two- and three-dimensional space [37]. The cubic spline function defined in Eq. (13) is a non-negative, monotonically decreasing function, and it is smooth at both the origin and the cutoff.

One way of obtaining particle–particle interactions with the required short-range repulsive and long-range attractive form is to use a sum of spline functions multiplied by an interaction strength coefficient a,

$$U(r) = a(AW_1(r) - BW_2(r)) = a(AW_1(r, r_{c1}) - BW_2(r, r_{c2})), \tag{14}$$

to define the particle–particle interaction potentials, where $W_1(r)$ is a cubic spline with a cutoff length of r_{c1}, A is the coefficient for $W_1(r)$, $W_2(r)$ is a cubic spline with a cutoff length of r_{c2} and B is the coefficient for $W_2(r)$. Here $W_1(r)$ and $W_2(r)$ are unnormalized shape functions given in Eq. (13). The DPD conservative particle–particle interaction forces are given by

$$F_{ij}^{C} = \frac{-\mathrm{d}U(r)}{\mathrm{d}\mathbf{r}}\hat{\mathbf{r}}_{ij}. \tag{15}$$

A variety of functions can be obtained using different combinations of A, r_{c1}, B, and r_{c2}. For example, if $A = 2.0$, $r_{c1} = 0.8$ and $B = 1.0$, $r_{c2} = 1.0$, and $a = 1$ (see Eq. (14)), the resulting potential function, $U(r) = AW_1(r) - BW_2(r)$ shown in Fig. 1, has both positive and negative components. The figure shows that the function $U(r)$ is positive at the origin, gradually decreases, and then becomes negative at $r = 0.4529$. After reaching the minimum, $U(r)$ increases until $U(r) = 0$ at $r = 1.0$. $U(r)$ is smooth at both the origin and at the point $r = 1.0$. If $A = 1.0$, $r_{c1} = 1.0$ and $B = 0.0$, the resulting potential function $U(r)$ is the cubic spline expressed in Eq. (13), which is non-negative everywhere (see Fig. 2).

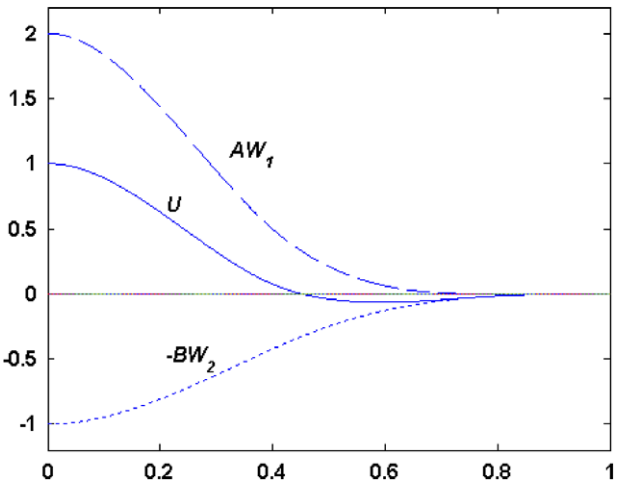

Fig. 1. Construction of a particle–particle interaction potential, $U(r)$, that is repulsive at short distances, attractive at intermediate distances and zero at large particle separation, from two cubic spline functions, $AW_1(r)$ and $BW_2(r)$.

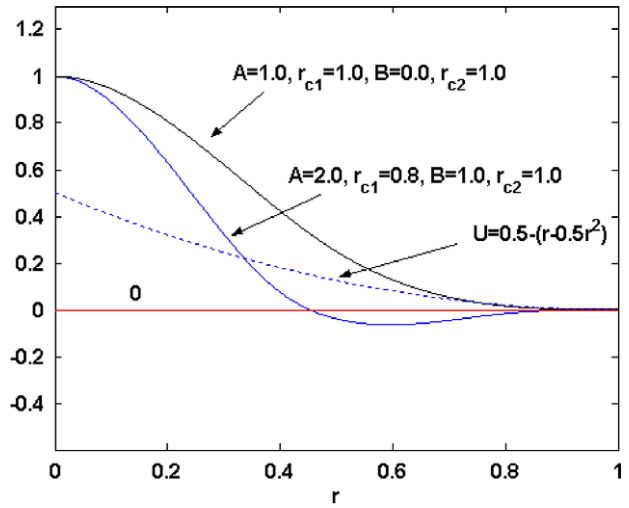

Fig. 2. Cubic spline potential functions, $U(r) = W_1(r, 1.0)$, $U(r) = 2W_1(r, 0.8) - W_2(r, 1.0)$ and the conventional DPD potential function, $U(r) = 0.5 - (r - 0.5r^2)$.

The cubic spline function $W(r)$ describes a purely repulsive interaction and its negative counterpart $-W(r)$ describes a purely attractive interaction. The parameters A and B determine the relative strengths of the repulsive and attractive interactions. Together with the interaction coefficient a, different A and B with corresponding cutoff distances r_{c1} and r_{c2} generate different potential functions, $U(r)$, and corresponding conservative force weight functions w^C ($w^C = -U'(r)$), which can be used to simulate different DPD materials. Once $U(r)$ and w^C are determined, physical parameters such as surface tension and transport coefficients of the concerned fluid can be numerically calculated [36]. Qualitatively, increasing the influence of the attractive component (increasing B) can increase the cohesion between the fluid particles, and therefore can result in bigger surface tension and physical viscosity. For a DPD system with attractive and repulsive interactions, the pressure–density relation can be numerically calculated via the virial theorem. The pressure–density relationship obtained using with attractive and repulsive interactions was shown to be consistent with the van der Waals equation (within the uncertainties inherent in the stochastic DPD modeling approach) [43].

Two SPH cubic spline potential functions $U(r) = 2W_1(r, 0.8) - W_2(r, 1.0)$ ($A = 2.0$, $r_{c1} = 0.8$, $B = 1.0$, $r_{c2} = 1.0$ and $a = 1.0$) and $U(r) = W_1(r, 1.0)$ ($A = 1.0$, $r_{c1} = 1.0$, $B = 0.0$ and $a = 1.0$) as well as the conventional potential function $0.5 - (r - 0.5r^2)$ (corresponding to the conventional weight function $1 - r$) are shown in Fig. 2. The corresponding force weight functions are shown in Fig. 3. Fig. 3 shows that the conventional DPD weight function is non-negative and corresponds to a purely repulsive interaction. Similarly, the weight function obtained using $A = 1.0$, $r_{c1} = 1.0$, $B = 0.0$ is non-negative function corresponding to a purely repulsive interaction. While the weight function obtained using $A = 2.0$, $r_{c1} = 0.8$, $B = 1.0$ and $r_{c2} = 1.0$ has positive and negative sections, which correspond to an interaction with short-range repulsive and long-range attractive characteristics. The derivatives of interaction potentials constructed from SPH cubic splines are zero at both the origin and the cutoff. Consequently, the interactions forces are smoother than those used in the standard DPD model.

The combination of the attractive and repulsive interactions in the cubic spline potential makes it possible to simulate systems with co-existing liquid and gas phases and liquid–gas phase transitions. The validity of the DPD method with long-range attractive and short-range repulsive particle–particle interactions in simulating multiphase flows has been verified by a series of numerical examples. One of them is the DPD simulation of the large-amplitude oscillations of an initially oblate liquid drop, which is driven by surface tension [43]. The DPD simulation results agree quite well with those obtained using smoothed particle hydrodynamics for a van der Waals fluid [44], and the experimental observations in the space shuttle Columbia in studying the oscillations of a large ball of water under micro gravity conditions [45].

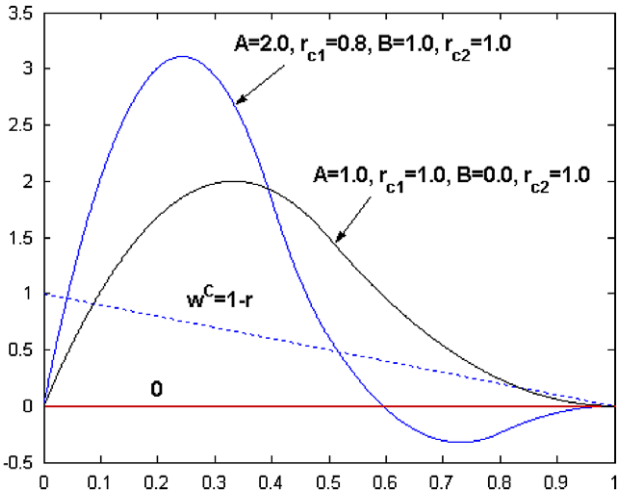

Fig. 3. Cubic spline conservative force weight functions and the conventional DPD conservative force weight function.

2.3. No-slip boundary condition

In DPD simulations, the effects of solid walls can be simulated by using fixed particles, which interact with the fluid particles. A convenient implementation is to fill the computational domain with particles, carry out a DPD simulation to equilibrate the particles, then 'freeze' the particles in the regions occupied by the solid walls and remove the remaining particles. Some of the mobile particles that are used to represent the fluid(s) may penetrate the wall particles because of the soft interaction between the DPD particles. One possible solution is to use higher particle density for the walls or a larger repulsive force between the wall particles and fluid particles.

Following Revenga et al. [38], we used a reflective boundary in addition to the interactions between fluid and wall particles. Revenga et al. investigated three different reflection models: (a) only the normal velocity component is reversed, (b) all velocity components are reversed, and (c) Maxwellian reflections where the particles are introduced back into the system with a Maxwell distribution of velocities. In our implementation of the Maxwell distribution, the velocities of particles that enter a thin layer next to the wall are selected randomly from the Maxwell distribution at temperature T, with a zero mean corresponding to the zero fluid velocity at the boundary. The velocity components are reversed if the velocity points outward from the bulk fluid. This treatment of solid boundaries by using frozen boundary particles and a thin reflecting boundary layer was found to be an effective way of implementing no slip boundary conditions [34].

The thickness of the thin layer is selected to ensure that the probability of penetration is very low but to occupy as little as possible of the fluid domain. In this work, the thickness of the boundary layer was 0.1 DPD units. This thickness is small compared with the size of the fluid domain so it does not affect the bulk flow and it allows the fluid and wall particles to interact strongly enough to control the wetting behavior. On the other hand, it is large enough to prevent unphysical penetration. The implementation of no-slip boundary conditions with frozen wall particles and a thin boundary layer was found to be very flexible, especially for problems with complex geometries such as flow in fractures.

3. Fluid motion between two smooth parallel walls

In this section, application of the DPD method and the cubic spline interaction functions to flow in the gap between two parallel plates (the most simple fracture aperture model) is described for two scenarios: fully saturated flow; and initially unsaturated flow with constant injection of fluid. The first case was used to validate the DPD method with the cubic spline potential by studying the hydrodynamic behavior of the DPD fluids. The second case was used to demonstrate that DPD with a combination of attractive and repulsive cubic

spline interaction potential functions can reproduce different flow modes within a simple fracture with flat walls.

3.1. Fully saturated flow within two parallel plates: Poiseuille flow

A DPD model with simple pairwise particle–particle interactions should conform to the Navier–Stokes equations on scales that are large enough for hydrodynamic (continuum) concepts to be valid (on scales large enough for the effects of both the discrete particle nature of the fluid, the mean free path of the particles and the thermal fluctuations to negligible), providing that the time step in the integration scheme approaches 0 [29]. The Poiseuille flow problem (flow between two parallel stationary infinite plates) has frequently been used to validate numerical methods. In Poiseuille flow, an initially stationary fluid, driven by a body force or a pressure gradient, flows between the two parallel plates, and finally reaches a steady state. In classical hydrodynamics, the flow velocity at a point between the two plates can be obtained by solving the Navier–Stokes equation or the Stokes equation if the Reynolds number is sufficiently low.

In a DPD simulation of Poiseuille flow, the entire flow domain is filled with DPD particles, and hence the flow can be regarded as a fully saturated flow in a simple fracture. The total number of particles depends on the size and geometry of the flow domain and the densities of the fluid and wall materials. The initial velocities of the particles were set randomly according to the given temperature but the wall particles were frozen. At the beginning of the simulation the particles were allowed to move without applying the external force until a thermodynamic equilibrium was reached. Then the external force field was applied to the fluid particles and the non-equilibrium simulation started.

A total of 20,640 particles of the same type were uniformly distributed at the sites of face centered cubic (FCC) lattice, which include 19,200 fluid particles in a flow domain of $40 \times 3 \times 40$ and 1440 wall particles located in three layers parallel to the (x, y) plane at each side. The number of particles corresponds to a density of 4.0 for both the fluid and wall particles. Periodic boundary conditions were used along both the x and y directions, while no-slip boundary condition was applied along the z direction. The coefficients used in the DPD simulation included: $a = 18.75$, $\sigma = 3.0$ and $k_B T = 1.0$ (hence $\gamma = 4.5$). A modified version of the velocity-Verlet algorithm [36] was used to simulate the particle dynamics, with $\lambda = 0.65$ and a time step of $\Delta t = 0.02$. A gravity force of $g = 0.02$ per particle (an acceleration of 0.02 for the particles of unit mass) was applied along the x direction, after the system reached equilibrium, to drive the flow. The system was divided into 200 bins along the z direction so that the temperature, velocity and density profiles, perpendicular to the direction of flow and the confining walls could be obtained by averaging the particle kinetic energies and particle velocities and determining the average particle density in each of these bins. The parameters associated with the cubic spline interaction potential were $A = 1.0$, $r_{c1} = 1.0$ and $B = 0.0$, $r_{c2} = 1.0$ ($U(r) = 18.75 W_1(r, 1.0)$). Hence this cubic spline potential does not have an attractive component.

Fig. 4 shows the temperature and density profiles along the z direction. The temperature calculated from the kinetic energy across the channel was uniform and remained almost equal to the initially specified temperature. The temperature variation is a direct measure of the accuracy of a DPD simulation. If a DPD simulation results in a kinetic temperature that differs significantly from the temperature calculated from Eq. (7), the simulation results will not be reliable. The density is also essentially uniform across the channel, except in the boundary region near the solid walls. The density fluctuations near the walls lead to pressure fluctuations near the walls, as shown in Fig. 5.

Fig. 6 shows the profile of the xz component of the stress tensor, Sxz. The DPD simulation results for Sxz agree well with the analytical solution $S_{xz} = -\rho g z$. Fig. 7 shows the profiles of the first normal stress difference ($N_1 = S_{xx} - S_{yy}$) and the second normal stress difference ($N_2 = S_{xx} - S_{zz}$) across the channel. Except for the regions near the wall, the two normal stress differences are close to zero compared with the shear stress.

Fig. 8 shows the development of the velocity profiles (velocity in the x direction) as the time increases. The velocity profile is fully developed (closely approaches the steady state profile) after about 80,000 steps (or 1600 DPD time units). For a Newtonian fluid, the asymptotic (long time limit) velocity profile at low Reynolds numbers obtained from the Navier–Stokes equation is $vx = V_{max}(1 - (\frac{z}{H})^2)$, where V_{max} is the maximum velocity in the x direction and H is half of the height of the channel (z direction). Fig. 9 shows the steady state velocity profile and the analytical solution with the same maximal velocity. This demonstrates that the velocity

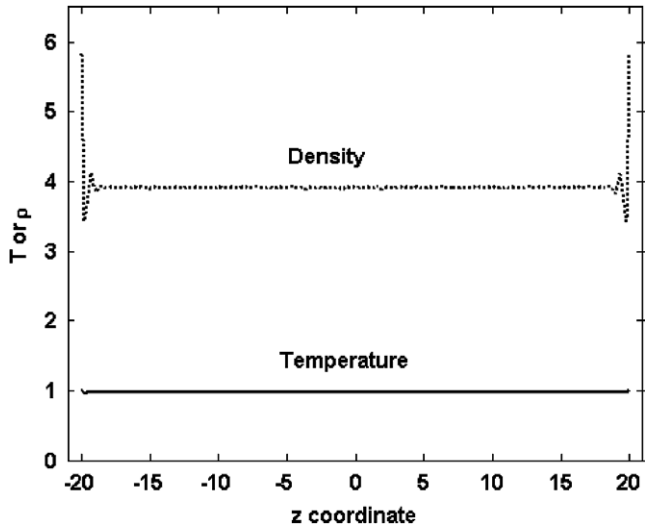

Fig. 4. The density and temperature profiles along the z direction.

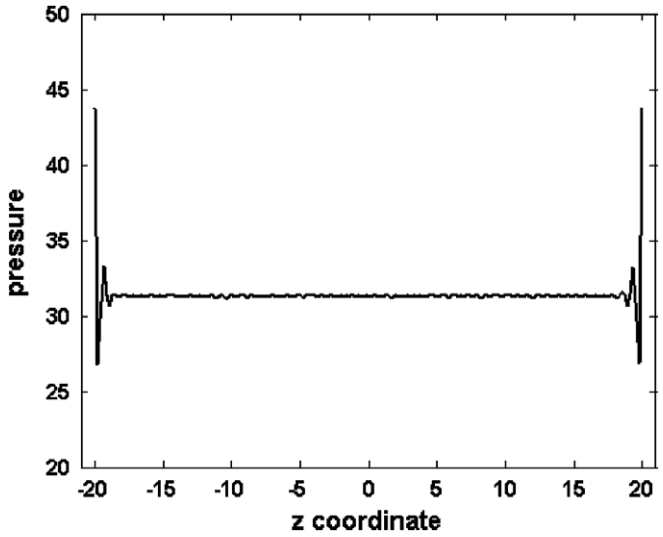

Fig. 5. The pressure profile in Poiseuille flow along the z direction.

profile obtained from the DPD simulation agrees well with the analytical solution of the Navier–Stokes equation. The good agreement between the measured and predicted profiles of the Sxz component of the stress tensor and the steady state velocity demonstrates that DPD simulations with the purely repulsive cubic spline particle–particle interaction energy function can successfully simulate fully saturated flow in a simple fracture and can reproduce the asymptotic (long length scale) hydrodynamic behavior embodied in the Navier–Stokes equation.

3.2. Unsaturated flow between parallel plates

In these simulations, DPD particles were randomly injected into the straight fracture at a constant injection rate. After equilibration, the DPD particles move into the aperture where they are influenced by each other, stationary wall particles and possibly external forces. If a purely repulsive interaction is used between the fluid particles, the injected particles will expand and occupy the whole fracture (the DPD fluid is a gas). If particle–

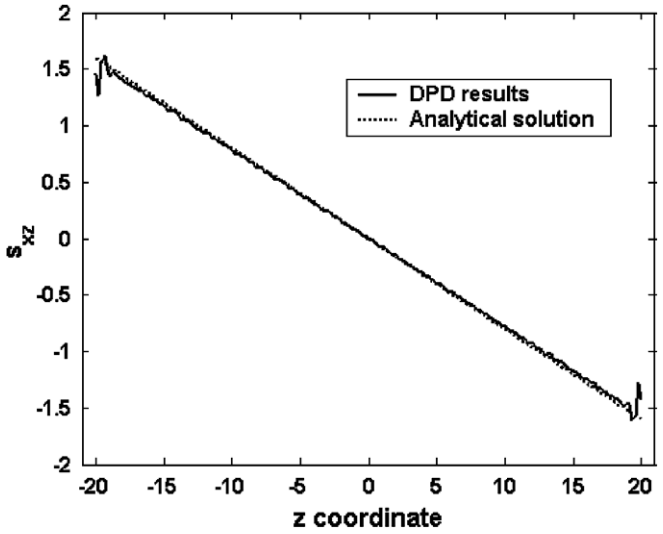

Fig. 6. The shear stress (Sxz) distribution along the z direction.

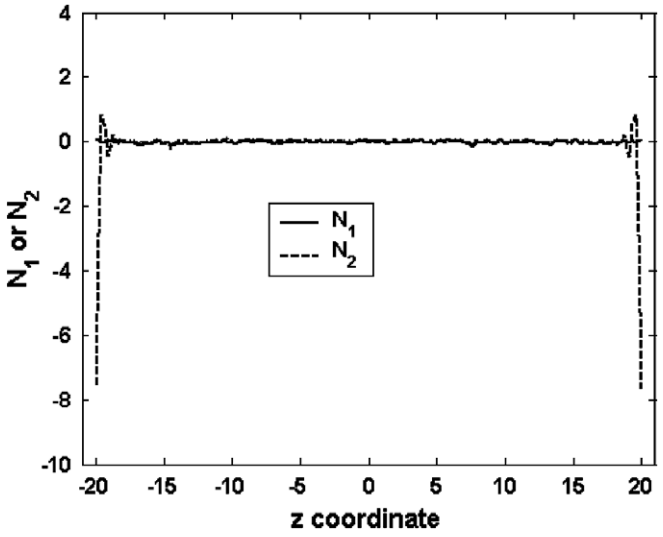

Fig. 7. Comparison of theoretical and simulated steady state velocity profiles (velocity in the x direction) across the channel.

particle interactions with short-range repulsion and long-range attraction are used, it is possible to simulate fluid flow with free surfaces, and flows with co-existing liquid and gas phases.

Unlike the simulation of single-phase fluid flow described in the previous example in which the wall particles were located at the sites of a regular FCC lattice, the simulations were carried out using walls that have a disordered internal structure. The DPD particles were randomly injected into a computational domain of $40 \times 3 \times 8$ until an average particle density of 4 was reached. After equilibration, the particles at the bottom and top edges, within one DPD unit of the boundaries, were frozen and became the stationary wall particles. The fluid particles were then randomly injected into the fracture at a pre-selected rate. The fluid particles were injected into the first column of DPD cells in the x direction at the left-hand side (Fig. 10), and particles that reached the opposite end of the system, at the maximum value of x, were removed. The injected particle equilibrated with the particles that had previously entered the aperture and the wall particles, and the injected fluid particles move to the right, further into the aperture, as the density of the injected particles and the concomitant pressure increased. A pressure drop along the fracture is produced due to the particle injection. The sur-

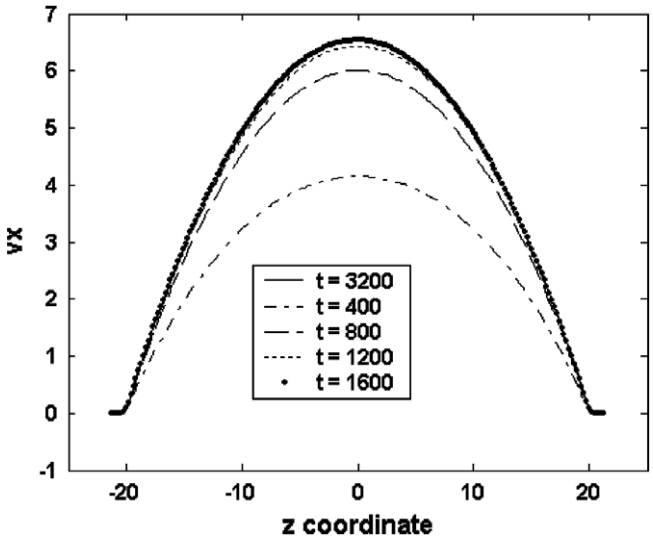

Fig. 8. The development of the velocity profiles (velocity in the x direction) across the channel.

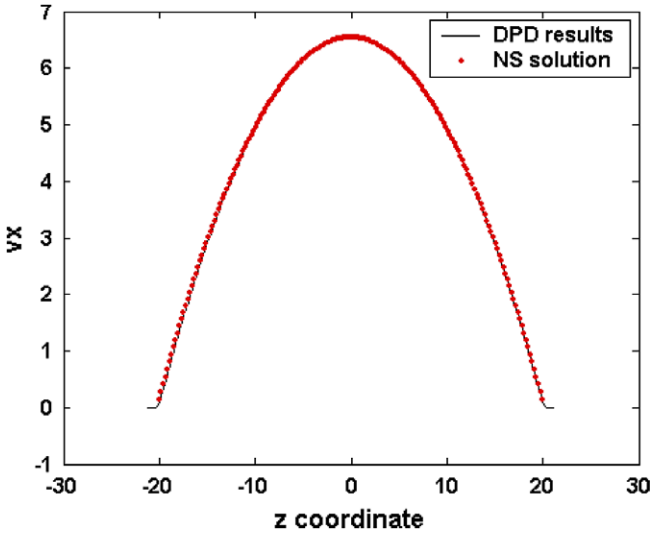

Fig. 9. The steady state velocity profiles (velocity in the x direction) across the channel.

face tension of the fluid is determined by the interplay between the attractive and repulsive components of the interaction between the fluid particles. The interaction between the wall particles and the fluid particles can be different from that between the fluid particles, and these interactions can be tuned to give different wetting behaviors and capillary forces. The pressure drop, surface tension, and wetting behavior or capillary force, together with possible external forces, govern the fluid flow in the fracture, which may exhibit a variety of flow regimes.

To simulate injection of fluid into the unsaturated fracture, periodic boundary condition was used along the y direction, and no-slip boundary conditions were applied on the fracture walls. The coefficients used in the DPD model were $\sigma = 3.0$ and $k_B T = 1.0$ ($\gamma = 4.5$). The interaction strength between the fluid particles was $a_f = 18.75$, while the interaction strength between the fluid and wall particles a_w was varied to mimic different wetting conditions. In the modified velocity-Verlet time integration algorithm, λ was 0.65, and a time step of $\Delta t = 0.02$ was used. A gravity force of $g = 0.02$ per particle was applied along the x direction, after the system reached equilibrium. The parameters for the SPH potential and weight function were $A = 2.0$, $r_{c1} = 0.8$ and

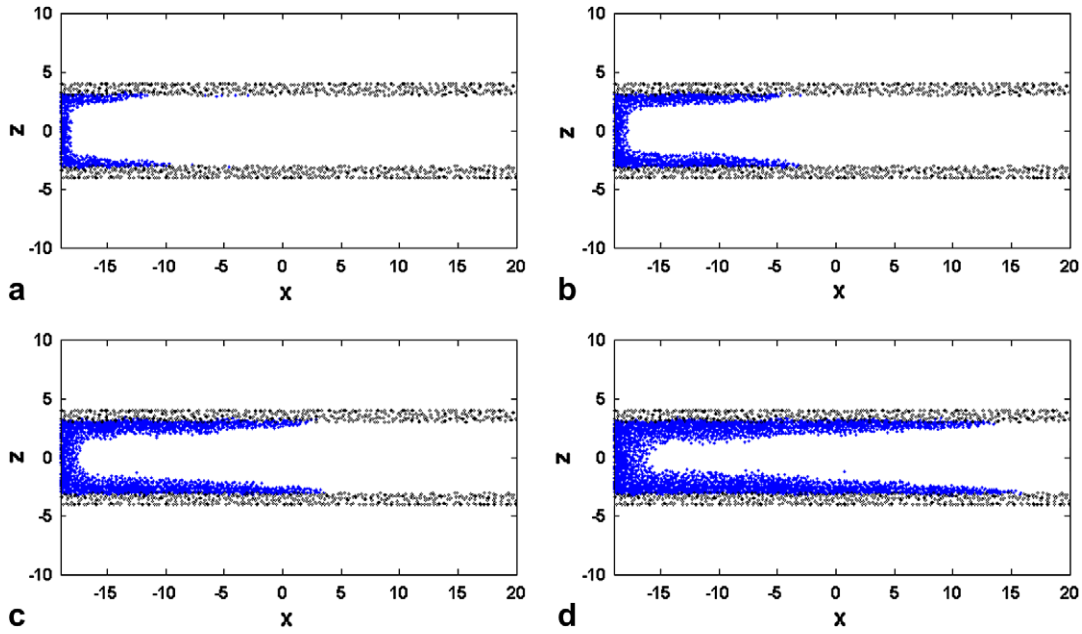

Fig. 10. Particle distributions during injection of strongly wetting fluid into the straight fracture at (a) 10,000, (b) 20,000, (c) 32,000, and (d) 55,000 steps. The injection rate was 10 particles per 100 steps, $a_w/a_f = 10.0$ and $g = 0.02$.

$B = 1.0$, $r_{c2} = 1.0$. Therefore the particle–particle interactions were given by $U(r) = a_f(2W_1(r, 0.8) - W_2(r, 1.0))$ for fluid–fluid particle interactions and $U(r) = a_w(2W_1(r, 0.8) - W_2(r, 1.0))$ for fluid–wall particle interactions.

The ratio between the interaction strengths, a_w/a_f, and the injection rate into the unsaturated fracture has a strong influence on the flow behavior. Fig. 10 illustrates a simulation with an injection rate of 10 particles per 100 steps, and a gravitational force of $g = 0.02$. The interaction ratio is 10 (the interaction between the wall and fluid particles is much larger than that between the fluid particles) and this generates strongly wetting behavior. The figure shows that the particles near the walls move into the aperture much faster than those far from the walls, and few particles evaporate from the bulk fluid. Because the positions of the frozen wall particles are disordered and the interactions between the fluid particles and other particles have a random component, the distribution of fluid particles is only roughly rather than perfectly symmetric. The contact angle is very small. In contrast to grid-based methods in which the contact angle is exactly imposed on the fluid, the contact angle in DPD studies is approximately estimated from the position of the wall and liquid particles. Further investigation revealed that a smaller injection rate or/and a larger interaction strength between the wall and fluid resulted in a smaller effective contact angle. This velocity dependent contact angle behavior is observed in real systems [39–42].

Fig. 11 shows a simulation of the injection of fluid into the unsaturated fracture with a particle injection rate of 100 particles per 100 steps and a gravitational force of $g = 0.02$. The interaction strength between the wall and fluid particles was 5 times the interaction strength between fluid particles. In this simulation the fluid propagates into the aperture with an approximately constant contact angle, which can be calculated from the shape of the advancing particle distributions. Again very few particles evaporated from the bulk flow. A larger injection rate or/and a smaller a_w ($a_w \geqslant a_f$) leads to a larger contact angle.

A convergence study was conducted for the two-phase injection flow through the unsaturated fracture. The convergence study is a little different from those in conventional grid-based methods and smoothed particle hydrodynamics. In grid-based methods and SPH, the convergence study is conducted by refining the mesh or increasing the overall number of particles so as to reduce the mass contained in each control volume a mesh element or a particle. In contrast, DPD simulation employs a DPD unit system in which all of the particles have equal masses and the mass of the particles is used as the unit of mass. It is not convenient to reduce the mass of each particle (away from unity) and therefore to increase the number of particles for an unchanged computational lattice system to examine the numerical convergence. Instead, since the length unit in a DPD

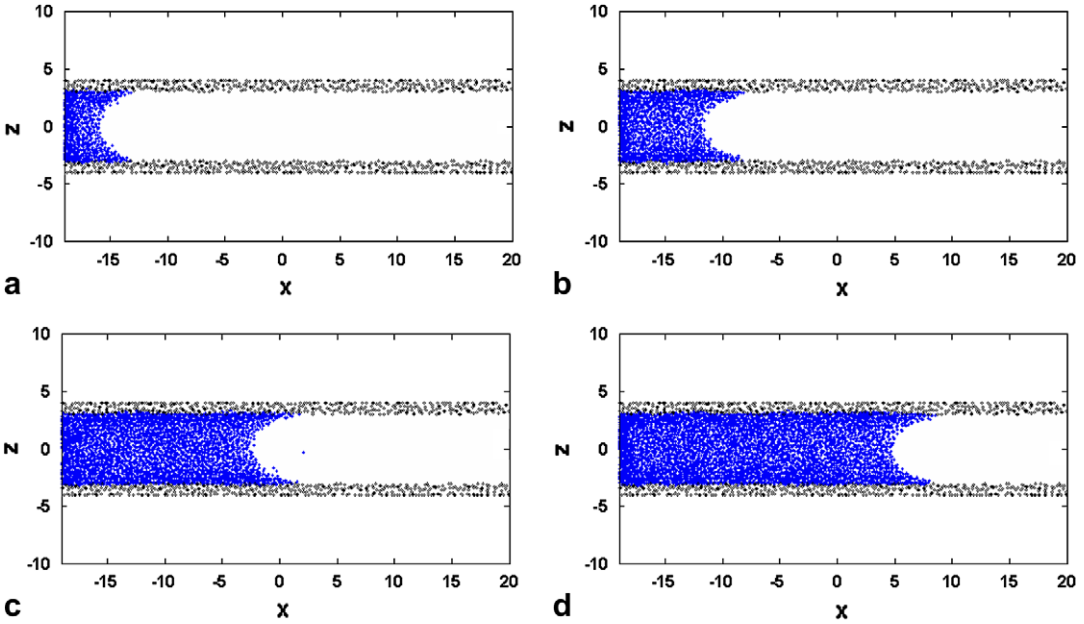

Fig. 11. Particle distribution during injection of wetting fluid into a straight fracture at (a) 1000, (b) 2100, (c) 4500, and (d) 6500 steps. The injection rate was 100 particles per 100 steps, $a_w/a_f = 5.0$ and $g = 0.02$.

simulation is also non-dimensional, it is convenient to enlarge the lattice system in DPD simulation (increase the number of DPD unit in each direction) and to reduce the ratio of DPD unit to the size of the real geometry so as to increase computational accuracy. Therefore the convergence study in DPD simulations can be implemented by using a larger lattice system with a larger number of DPD particles.

Two scenarios with lattice systems of 40×8 and 80×16, respectively, in x and z directions were simulated. In the two simulations, a gravitational force and interaction ratio were $g = 0.02$ and $a_w/a_f = 0.25$, respectively. The particle injection rate is 100 particles per 100 steps for the case with a lattice system of 40×8 in x and z directions and 400 particles per 100 steps for the case with enlarged lattice system. Fig. 12 shows the flow patterns for the two scenarios at four stages in a normalized non-dimensional configuration. The flow patterns obtained from two scenarios are very alike. Since the interaction strength between fluid particles is stronger than that between the fluid particles and wall particles, the contact angle is relatively large. Both scenarios demonstrate this non-wetting effect. The positions of the bulk fluid front obtained from the two scenarios are nearly the same. This shows that the obtained DPD simulation results are convergent (see Table 1).

Figs. 10–12 show that the DPD method with cubic spline interaction potential functions can produce film flow (strong wetting flow), wetting flow and non-wetting flow at different injection rates and different ratios of the interaction strengths.

4. Fluid motion through an unsaturated fracture junction

In this section, fluid motion through an unsaturated fracture junction is investigated using DPD with a combination of cubic spline interaction potential functions. The fracture junction has an inverted Y shape consisting of a vertical fracture that divides into two branch fractures with the same aperture (Fig. 13). The fluid dynamics in this type of fracture junction has recently been investigated experimentally [6,7].

The size of the computational domain was $80 \times 3 \times 80$. The walls of the branched fracture were represented by 2645 stationary particles using essentially the same procedure that was used for the simple parallel walled fracture. No-slip boundary conditions were used along the fracture walls, and particles were injected near the top of the vertical fracture. The coefficients used in the DPD model were $\sigma = 3.0$ and $k_B T = 1.0$ ($\gamma = 4.5$). The interaction strength between the fluid particles was $a_f = 18.75$, and a_w, the strength of the interactions between the fluid and wall particles can be changed to mimic different wetting behaviors. In the modified velocity-Ver-

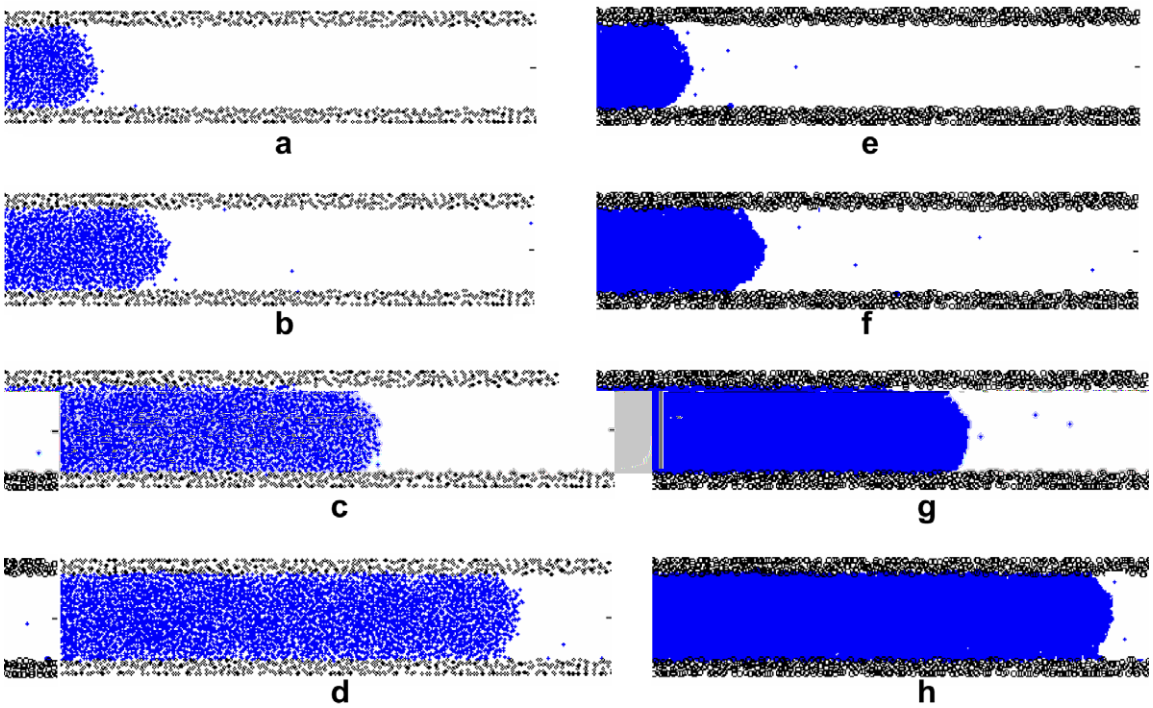

Fig. 12. Flow patterns of the injection of a non-wetting fluid into the straight fracture. The four figures in the left column (a–d) show the DPD simulation snapshots with a lattice system of 40×8 in x and z directions and the four figures in the right column (e–h) show the results with a lattice system of 80×16 at 1100, 2000, 4200, and 6200 steps.

Table 1
Position of the bulk fluid front in the channel

Time step	1100	2000	4200	6200
40×8	0.195	0.329	0.599	0.838
80×16	0.199	0.335	0.607	0.848

The positions of the bulk fluid front in the channel are normalized by the channel length.

let time integration algorithm, λ was set to 0.65, and the time step was set to $\Delta t = 0.02$. The parameters for the SPH potential and weight functions were $A = 2.0$, $r_{c1} = 0.8$, $B = 1.0$ and $r_{c2} = 1.0$. Again, the particle–particle interaction potentials were given by $U(r) = a_f(2W_1(r, 0.8) - W_2(r, 1.0))$ for fluid–fluid particle interactions and $U(r) = a_w(2W_1(r, 0.8) - W_2(r, 1.0))$ for fluid–wall particle interactions.

The fluid particles were injected into at the top of the vertical branch within 2 length units ($2r_c$) of the upper boundary, and after equilibration, the fluid particles moved downwards in the fracture. The pressure drop and capillary forces together with the effects of gravity acting on the fluid particles govern fluid flow in the fracture junction. By adjusting the ratio of interaction strengths a_w/a_f, the injection rate and the gravitational acceleration, different flow behaviors were simulated.

Fig. 14 illustrates a simulation with an injection rate of 100 particles per 100 steps, an interaction ratio a_w/a_f of 2, and a gravitational acceleration, g, of 0.01 (downwards in the z direction). This interaction ratio, a_w/a_f, leads to a relatively weak wetting effect with a contact angle that is large but smaller than $\pi/2$. Again, the particle distribution is roughly rather than perfectly symmetric, and only a few particles evaporate from the bulk fluid. The figure shows that before the bulk fluid reaches the fracture intersection, a stable concave meniscus is established, with a roughly constant contact angle (Fig. 14a and b). When the bulk fluid reaches the fracture junction, the curvature of the concave meniscus gradually decreases, and then becomes convex (Fig. 14b–d) due to effect of gravity acting on the accumulating mass of liquid above the meniscus. This transition from a concave meniscus to convex meniscus in the junction was observed experimentally and investigated analyt-

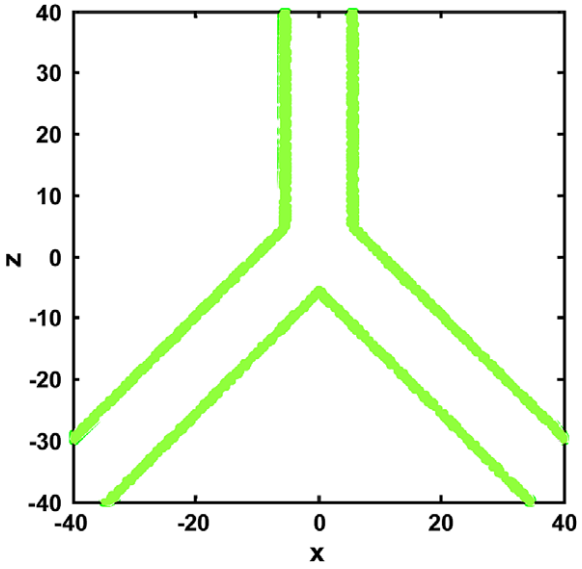

Fig. 13. Geometry of the simulated fracture intersection, which is similar to the experimental configuration used in [6,7].

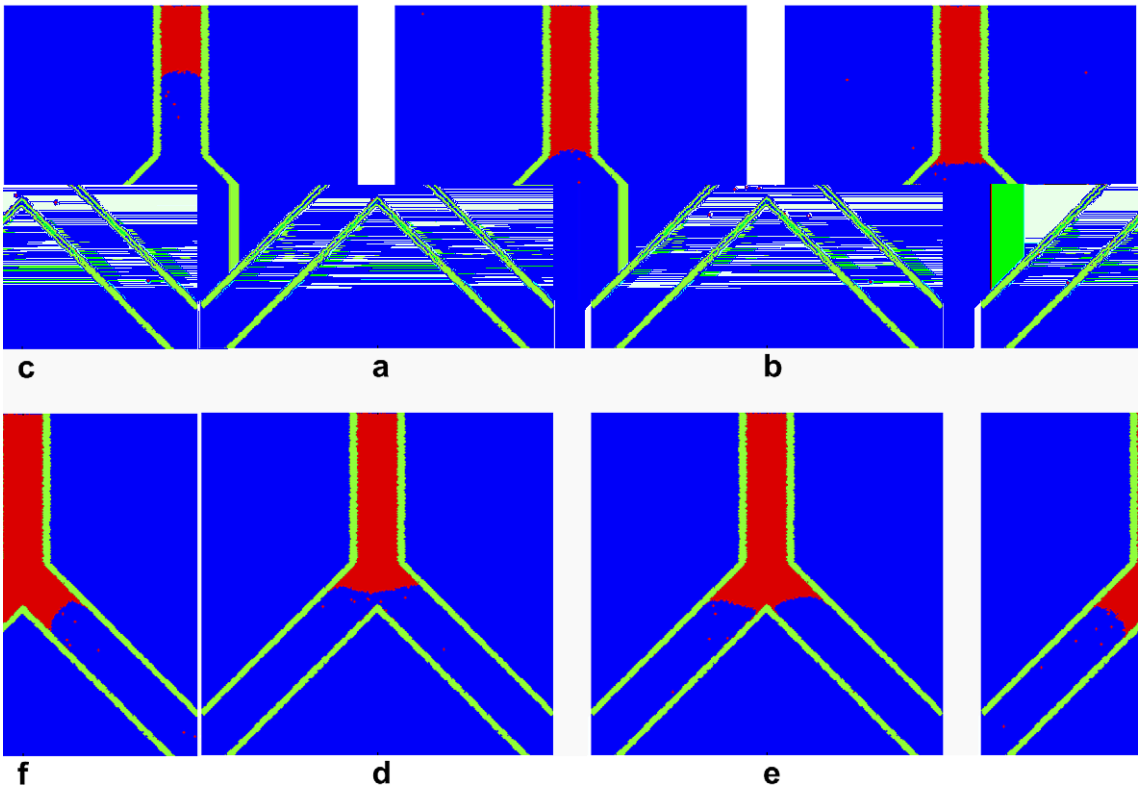

Fig. 14. Six stages during a simulation of fluid injection into a branched fracture at (a) 4800, (b) 10,800, (c) 11,800, (d) 14,300, (e) 16,700, and (f) 18,900 steps. The injection rate was 100 particles per 100 steps, $a_w = 2.0a_f$, and $g = 0.01$.

ically by Dragila and Weisbrod [6], although their analysis was based on an invading droplet rather than continuously injection of fluid. For a given injection rate and gravity force, the transition from a concave to a convex meniscus occurs at a lower liquid volume for a smaller interaction ratio a_w/a_f ($a_w/a_f \geqslant 1$) with a larger

contact angle. The convex meniscus moves downward gradually and then reaches the apex of the fracture junction (Fig. 14d). Once the bulk fluid arrives at the apex, the fluid flow divides into the two inclined branches and soon forms a concave meniscus in each inclined branch with a contact angle roughly equal to that formed previously in the vertical wall (Fig. 14e and f). It can be seen that the fracture junction is then fully saturated by the invading fluid.

Fig. 15 shows the distribution of DPD liquid at six stages during a simulation of liquid injection into the fracture junction with an injection rate of 50 particles per 100 steps, an interaction ratio a_w/a_f of 5, and a downward gravitational acceleration of 0.01. In this simulation, the fluid is strongly wetting, and the contact angle is very small. As in the previous case, a stable concave meniscus, with a roughly constant contact angle develops before the bulk fluid reaches the junction. However, the meniscus retains its concave shape as it moves through the junction. After the bulk fluid arrives at the apex, the fluid flow divides into the two branches and concave menisci develop in each branch, with a contact angle roughly equal to that formed earlier in the vertical wall. Again the fracture junction is fully saturated by the invading fluid.

If the injection rate is reduced or/and the interaction ratio is increased, a thin liquid films advances along the walls, ahead of the bulk fluid, due to the slower downward velocity of the bulk fluid (or failure to form bulk fluid spanning the aperture if the injection rate is too low) and stronger wetting of the fracture walls. Fig. 16 shows the development of film flow with an injection rate of 10 particles per 100 steps, an interaction strength ratio, a_w/a_f, of 10 and a downward gravitational force, g, of 0.01 per particle. It can be seen that the film flow occurs not only in the vertical fracture before the fracture junction, but also in the two fracture branches.

Fig. 17 shows the flow mode switching from a fully saturated flow mode to a thin film flow mode. The four figures in the upper row show the DPD simulation snapshots at (a) 10,000, (b) 20,000, (c) 60,000, and (d) 7000 steps. The four figures in the lower row show the VOF results at (e) $t = 0.04$ s, (f) $t = 0.08$ s, (g) $t = 0.24$ s and (h) $t = 0.28$ s. Since the DPD unit is non-dimensional, the time step in the DPD simulation can be related to

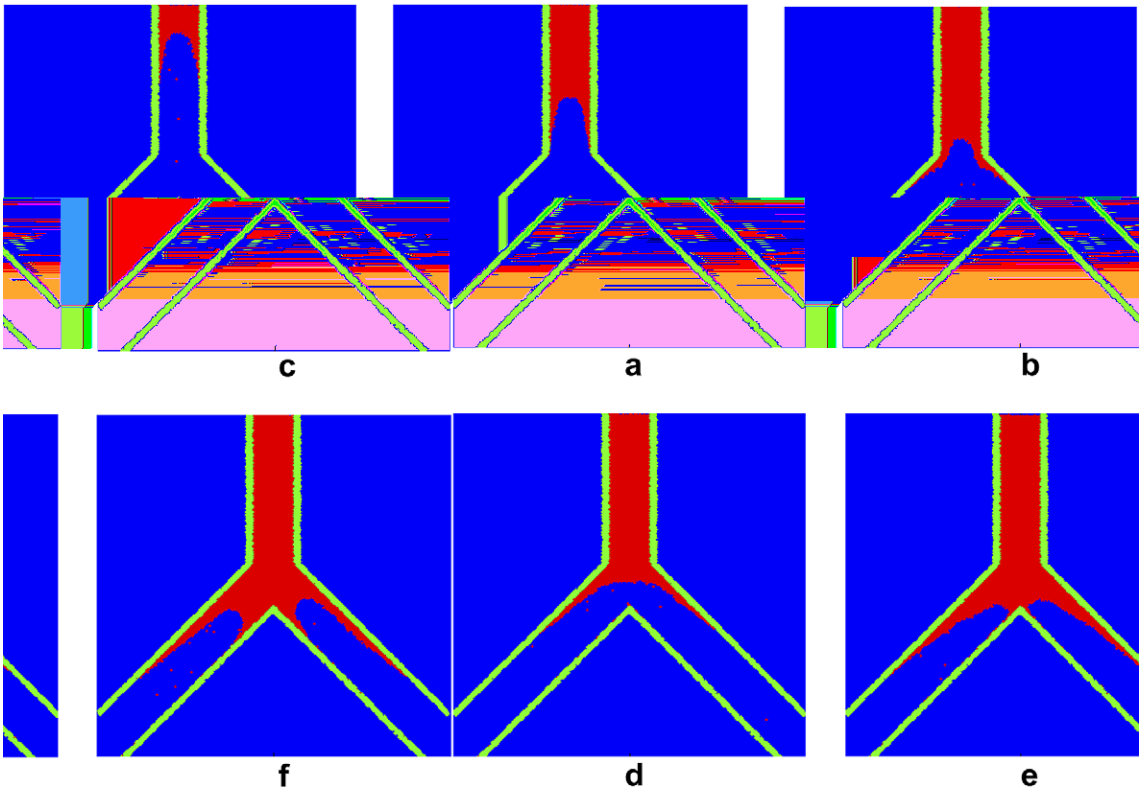

Fig. 15. Six stages in a simulation of injection into an unsaturated fracture junction at (a) 7000, (b) 18,200, (c) 25,500, (d) 34,000, (e) 45,500, and (f) 47,500 steps. The injection rate was 50 particles per 100 steps, $a_w = 5.0a_f$, and $g = 0.01$.

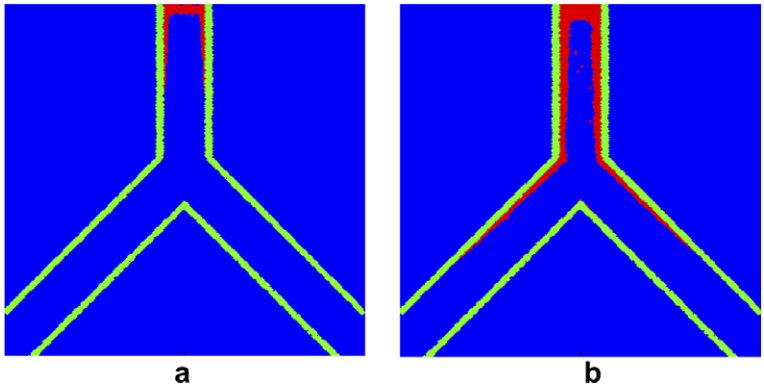

Fig. 16. Six stages in a simulation of fluid injection into an unsaturated fracture junction at (a) 30,000, and (b) 130,000 steps. The injection rate was 10 particles per 100 steps, $a_w = 10.0a_f$, and $g = 0.01$.

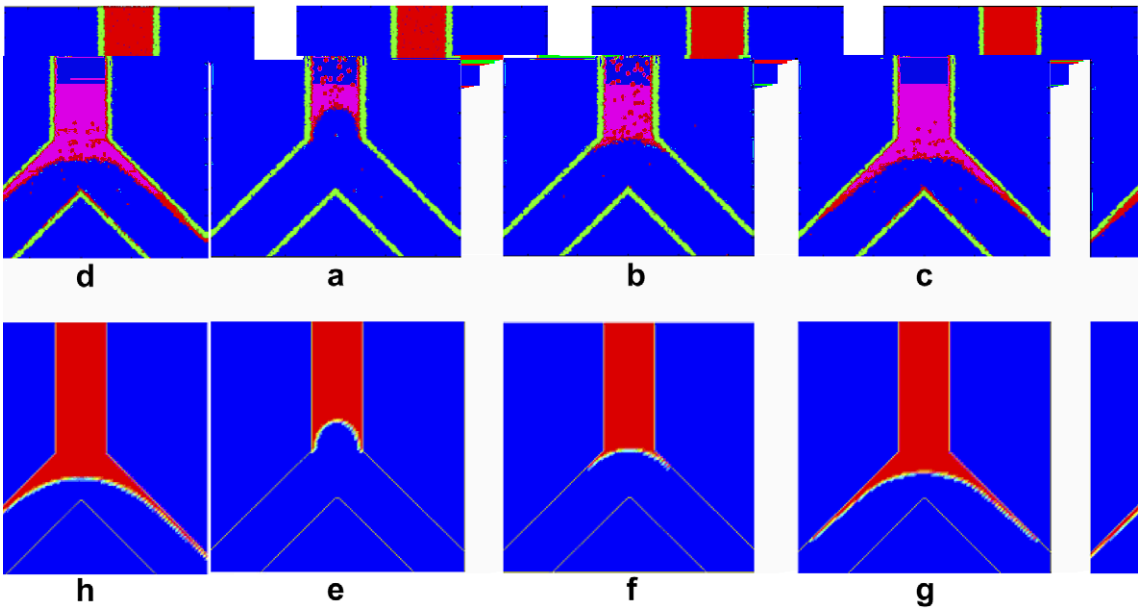

Fig. 17. Simulations of flow mode switching from a fully saturated flow to a thin film flow using DPD and VOF model at a small contact angle. The four figures in the upper row show the DPD simulation snapshots at (a) 10,000, (b) 20,000, (c) 60,000, and (d) 7000 steps. The four figures in the lower row show the VOF results at (e) $t = 0.04$ s, (f) $t = 0.08$ s, (g) $t = 0.24$ s and (h) $t = 0.28$ s.

physical time if a proper scale is used. One straightforward approach is to calculate the ratios of the simulated DPD time steps in the DPD simulation, and the ratios of the physical time instants in the VOF simulation. If the ratios are comparable, the non-dimensional DPD time can be regarded as equivalent to the VOF physical time. It is clear that in Fig. 17, the DPD simulation snapshots at (a) 10,000, (b) 20,000, (c) 60,000, and (d) 7000 steps and the VOF snapshots at (e) $t = 0.04$ s, (f) $t = 0.08$ s, (g) $t = 0.24$ s and (h) $t = 0.28$ s are at equivalent stages as both were associated with ratios of 1, 2, 6 and 7, respectively.

The parameters used in the DPD simulation were $A = 2.0$, $r_{c1} = 0.8$, $B = 1.0$, and $r_{c2} = 1.0$. At the start of the simulation, 90% of the vertical fracture from top side is fully saturated and 10% is unsaturated. The fluid particles move downward, and then separate into the two branch fractures due to the pressure generated by particle injection, surface tension, and wetting behavior. The injection rate was 10 particles per 100 steps, the interaction strength for the two branch fracture walls was $a_w = 10.0a_f$ and the downward gravitational force was $g = 0.01$. Due to the strong wettability of the fracture wall in the two branches, a thin film extends along

the wall of the fracture junction, and then moves rapidly into the two divided branches. Though the vertical wall above the fracture junction is fully saturated at the later stages, the fracture junction is only partially saturated eventually. Although the film flow keeps moving forward, the concave meniscus in the fracture junction maintains nearly the same shape as a steady meniscus (Fig. 17c and d). The contact angle for the thin film flow is very small ($<2°$). The DPD simulation captures major physics in the flow mode switching dynamics, which was also observed by Dragila and Weisbrod [6] for an invading droplet.

This flow mode switching process is difficult to simulate for most conventional grid-based numerical methods. Huang et al. developed a volume of fluid (VOF) model which is capable of investigating unsaturated multiphase flow through fracture networks [46]. The presented VOF model can handle fragmentation and merging of liquid interfaces automatically without resorting to adaptive mesh refinement or interface repairing algorithms. Wetting effects can be modeled by imposing dynamic contact angles near the contact line, and different contact angles can be automatically chosen, depending on whether the liquid interface is advancing, receding or essentially stationary. This VOF model was also used to simulate the flow mode switching process. The surface tension, dynamic viscosity, and density for the simulated fluid were 0.0728 N/m; 1.52×10^{-3} (N s)/m^2; and 1000 kg/m^3, respectively, and the gravitational acceleration was 9.8 m/s^2. These fluid properties are similar to those of water under normal conditions. A number of grid resolutions were tried to test the convergence of the VOF simulation. Fig. 17 shows the convergent VOF simulation results with an imposed advancing contact angle of 1°, and a grid size of 100×100. The flow pattern obtained using DPD simulation also agrees well with that obtained using a VOF model, which was proven to be effective in simulating complex flow dynamics in fracture junction and fracture networks.

5. Conclusions

A purely repulsive pairwise particle–particle interaction model has been frequently used in dissipative particle dynamics to simulate the behavior of a gas. In this paper, we show that a single component two-phase (liquid–gas) fluid or a liquid with a free surface can be simulated by using a combination of short range repulsive and long range attractive particle–particle interactions. To illustrate this approach for simulating multiphase fluid behavior we used a particle–particle interaction potential model derived from cubic spline SPH weighting functions. In general, it can be expected that DPD simulations with this type of interaction potential can be used to simulate gasses, liquids, solids and multiphase systems, depending on the average particle density, the temperature and the details of the particle–particle interactions.

Dissipative particle dynamics with a combination of short range repulsive and (relatively) long range attractive components was used to simulate multiphase flow in simple fractures and fracture junctions, which usually involve complex flow dynamics arising from moving interface and/or large density/viscosity ratios. It was demonstrated that DPD with a purely repulsive SPH like weight function can successfully model fully saturated flow in a simple fracture aperture consisting of the gap between two parallel plates and can reproduce the hydrodynamic behavior predicted by the Navier–Stokes equation. Injection of DPD fluid into an unsaturated fracture resulted in different flow modes, including film flow, wetting and non-wetting flow under various injection rates and the fluid–fluid and fluid–wall interaction strengths, and external forces.

For the injection of DPD fluid into an unsaturated fracture junction with a vertical fracture that divides symmetrically into two inclined fractures, different flow modes were also observed depending on the injection rate, fluid–fluid and fluid–wall interaction strengths, and external forces.

Acknowledgment

This work was supported by the US Department of Energy's Environmental Management Science Program under contract DE-AC07-05ID14517 at the Idaho National Laboratory.

References

[1] R. Nativ, E. Adar, O. Dahan, M. Geyh, Water recharge and solute transport through the vadose zone of fractured chalk under desert conditions, Water Resour. Res. 31 (2) (1995) 253.

[2] I.C. Yang, G.W. Rattray, P. Yu, Interpretations of chemical and isotopic data from boreholes in the unsaturated-zone at Yucca Mountain, Nevada, U.S. Geological Survey Water-Resources Investigation Report 96-4.58, 1996.
[3] J.T. Fabryka-Martin, P.R. Dixon, S.S. Levy, B. Liu, D.L. Brenner, L.E. Wolfsberg, H.J. Turin, P. Sharma, Implications of environmental isotopes for flow and transport in the unsaturated zone at Yucca Mountain, Nevada, Geol. Soc. Am. Abstr. Programs 28 (7) (1996) A-416.
[4] B.R. Scanlon, S.W. Tyler, P.J. Wierenga, Hydrologic issues in arid, unsaturated systems and implications for contaminant transport, Rev. Geophys. 35 (4) (1997) 461.
[5] National Research Council (NRC), Conceptual Models of Flow and Transport in the Fractured Vadose Zone, Notational, Academic Press, Washington, DC, 2001.
[6] M.I. Dragila, N. Weisbrod, Fluid motion through an unsaturated fracture junction, Water Resour. Res. 40 (2004) W02403, doi:10.1029/2003WR002588.
[7] M.I. Dragila, N. Weisbrod, Parameters affecting maximum fluid transport in large aperture fractures, Adv. Water Resour. 26 (2003) 1219.
[8] E.M. Kwicklis, R.W. Healy, Numerical investigation of steady liquid water flow in a variably saturated fracture network, Water Resour. Res. 29 (12) (1993) 4091.
[9] P. Persoff, K. Pruess, Two-phase flow visualization and relative permeability measurement in natural rough-walled rock fractures, Water Resour. Res. 31 (5) (1995) 1175.
[10] K. Pruess, Two-phase unsaturated flow at Yucca Mountain, Nevada: a report on current understanding, second ed., in: D.D. Evans, T.J. Nicholson, T.C. Rasmussen (Eds.), Flow and Transport Through Unsaturated Fractured Rock, Geophysics Monograph Series, vol. 42, AGU, Washington, DC, 2001, pp. 113–133.
[11] F.H. Harlow, The particle-in-cell computing method for fluid dynamicsMethods in Computational Physics, Fundamental Methods in Hydrodynamics, vol. 3, Academic Press, New York, 1964.
[12] S.O. Unverdi, G. Tryggvason, A front-tracking method for viscous, incompressible, multi-fluid flows, J. Comput. Phys. 100 (1992) 25.
[13] C.W. Hirt, B.D. Nichols, Volume of fluid method (VOF) for the dynamics of free boundaries, J. Comput. Phys. 39 (1981) 201.
[14] M. Sussman, P. Smereka, S. Osher, A level set approach for computing solutions to incompressible two-phase flow, J. Comput. Phys. 114 (1994) 146.
[15] S. Succi, The Lattice Boltzmann Equation for Fluid Dynamics and Beyond, Clarendon Press, Oxford, 2001.
[16] D.H. Rothman, S. Zaleski, Lattice Gas Cellular Automata: Simple Models for Complex Hydrodynamics, Cambridge University Press, Cambridge, 1997.
[17] J.P. Rivet, J.P. Boon, Lattice Gas Hydrodynamics, Cambridge University Press, Cambridge, 2000.
[18] A.J.C. Ladd, Numerical simulations of particulate suspensions via a discretized Boltzmann equation. part 1. Theoretical foundation, J. Fluid Mech. 271 (1994) 285.
[19] H.W. Stockman, C.H. Li, J.L. Wilson, A lattice-gas and lattice Boltzmann study of mixing at continuous fracture junctions: importance of boundary conditions, Geophys. Res. Lett. 24 (12) (1997) 1515.
[20] R.A. Gingold, J.J. Monaghan, Smoothed particle hydrodynamics: theory and application to non-spherical stars, Mon. Not. R. Astron. Soc. 181 (1977) 375–389.
[21] J.J. Monaghan, Smoothed particle hydrodynamics, Annu. Rev. Astron. Astr. 30 (1992) 543–574.
[22] L.B. Lucy, Numerical approach to testing of fission hypothesis, Astron. J. 82 (1977) 1013–1024.
[23] A.M. Tartakovsky, P. Meakin, Modeling of surface tension and contact angles with smoothed particle hydrodynamics, Phys. Rev. E 72 (2005) 026301.
[24] A.M. Tartakovsky, P. Meakin, A smoothed particle hydrodynamics model for miscible flow in three-dimensional fractures and the two-dimensional Rayleigh–Taylor instability, J. Comput. Phys. 207 (2005) 610.
[25] P.J. Hoogerbrugge, J.M.V.A. Koelman, Simulating microscopic hydrodynamic phenomena with dissipative particle dynamics, Europhys. Lett. 19 (3) (1992) 155.
[26] I. Pagonabarraga, D. Frenkel, Dissipative particle dynamics for interacting systems, J. Chem. Phys. 115 (11) (2001) 5011.
[27] P. Español, P. Warren, Statistical mechanics of dissipative particle dynamics, Europhys. Lett. 30 (4) (1995) 191.
[28] R. Kubo, Fluctuation–dissipation theorem, Rep. Prog. Phys. 29 (1966) 255–284.
[29] C. Marsh, Theoretical aspect of dissipative particle dynamics, Ph.D. Thesis, University of Oxford, 1998.
[30] J.M.V.A. Koelman, P.J. Hoogerbrugge, Dynamics simulation of hard-sphere suspensions under steady shear, Europhys. Lett. 21 (1993) 363.
[31] R.R. Groot, Mesoscopic simulation of polymer-surfactant aggregation, Langmuir 16 (2000) 7493.
[32] A.G. Schlijper, P.J. Hoogerbrugge, C.W. Manke, Computer simulation of dilute polymer solutions with the dissipative particle dynamics method, J. Rheol. 39 (1995) 567.
[33] R.D. Groot, K.L. Rabone, Mesoscopic simulation of cell membrane damage, morphology change and rupture by nonionic surfactants, Biophys. J. 81 (2001) 725.
[34] X.J. Fan, P.T. Nhan, T.Y. Ng, X.H. Wu, D. Xu, Microchannel flow of a macromolecular suspension, Phys. Fluids 15 (1) (2003) 11.
[35] J.H. Irving, J.G. Kirkwood, The statistical mechanics of transport process IV. The equation of hydrodynamics, J. Chem. Phys. 18 (1950) 817.
[36] R.D. Groot, P.B. Warren, Dissipative particle dynamics: bridging the gap between atomic and mesoscopic simulation, J. Chem. Phys. 107 (11) (1997) 4423.
[37] M.B. Liu, G.R. Liu, K.Y. Lam, Constructing smoothing functions in smoothed particle hydrodynamics with applications, J. Comput. Appl. Math. 155 (2) (2003) 263.

[38] M. Revenga, I. Zuñiga, P. Español, Boundary models in DPD, Int. J. Mod. Phys. C 9 (8) (1998) 1319.
[39] P.G. deGennes, Wetting: statics and dynamics, Rev. Mod. Phys. 57 (1985) 827–863.
[40] R.G. Cox, Inertial and viscous effects on dynamic contact angles, J. Fluid Mech. 357 (1998) 249–278.
[41] R.A. Hayes, J. Ralston, Forced liquid movement on low-energy surfaces, J. Colloid Interf. Sci. 159 (2) (1993) 429–438.
[42] R.L. Hoffman, Study of advancing interface. 1. Interface shape in liquid–gas systems, J. Colloid Interf. Sci. 50 (2) (1975) 228–241.
[43] M.B. Liu, P. Meakin, H. Huang, Dissipative particle dynamics with attractive and repulsive particle–particle interactions, Phys. Fluids 18 (2006) 017101.
[44] R.E. Apfel, Y. Tian, J. Jankovsky, T. Shi, X. Chen, R.G. Holt, E. Trinh, A. Croonquist, K.C. Thornton, A. Sacco Jr., C. Coleman, F.W. Leslie, D.H. Matthiesen, Free oscillations and surfactant studies of sperdeformed drops in microgravity, Phys. Rev. Lett. 78 (1977) 1912.
[45] S. Nugent, H.A. Posch, Liquid drops and surface tension with smoothed particle applied mechanics, Phys. Rev. E. 62 (2000) 4968.
[46] H. Huang, P. Meakin, M.B. Liu, G.E. McCreery, Modeling of multiphase fluid motion in fracture intersections and fracture networks, Geophys. Res. Lett. 32 (2005) L19402, doi:10.1029/2005GL023899.